Virology **271,** 321–333 (2000)
doi:10.1006/viro.2000.0321, available online at http://www.idealibrary.com on IDEAL®

Molecular Architecture of Bacteriophage T4 Capsid: Vertex Structure and Bimodal Binding of the Stabilizing Accessory Protein, Soc

Kenji Iwasaki,* Benes L. Trus,*,† Paul T. Wingfield,‡ Naiqian Cheng,*
Gregorina Campusano,*,§ Venigalla B. Rao,*,§ and Alasdair C. Steven*,[1]

*Laboratory of Structural Biology and ‡Protein Expression Laboratory, National Institute of Arthritis, Musculoskeletal and Skin Diseases; †Computational Bioscience and Engineering Laboratory, Center for Information Technology, National Institutes of Health, Bethesda, Maryland 20892; and §Department of Biology, The Catholic University of America, Washington, DC 20064

Received February 7, 2000; accepted March 14, 2000

T4 encodes two dispensable proteins that bind to the outer surface of the mature capsid. Soc (9 kDa) stabilizes the capsid against extremes of alkaline pH and temperature, but Hoc (40 kDa) has no perceptible effect. Both proteins have been developed as display platforms. Their positions on the hexagonal surface lattice of gp23*, the major capsid protein, were previously defined by two-dimensional image averaging of negatively stained electron micrographs of elongated variant capsids. We have extended these observations by reconstructing cryo-electron micrographs of isometric capsids produced by a point mutant in gene 23, for both Hoc+.Soc+ and Hoc+.Soc− phages. The expected T = 13 lattice was observed, with a single Hoc molecule at the center of each gp23* hexamer. The vertices are occupied by pentamers of gp24*: despite limited sequence similarity with gp23*, the respective monomers are similar in size and shape, suggesting they may have the same fold. However, gp24* binds neither Hoc nor Soc; *in situ*, Soc is visualized as trimers at the trigonal points of the gp23* lattice and as monomers at the sites closest to the vertices. In solution, Soc is a folded protein (~10% α-helix and 50–60% β sheet) that is monomeric as determined by analytic ultracentrifugation. Thus its trimerization on the capsid surface is imposed by a template of three symmetry-related binding sites. The observed mode of Soc binding suggests that it stabilizes the capsid by a clamping mechanism and offers a possible explanation for the phenotype of osmotic shock resistance.

Key Words: Cryo-electron microscopy; bacteriophage assembly; virus structure; phage display; quasi-equivalence; osmotic shock resistance.

INTRODUCTION

The study of bacteriophage assembly has disclosed regulatory mechanisms pertinent not only to viruses but to macromolecular complexes in general. Of the well-characterized dsDNA phages, T4 has the largest and most complex capsid, some 20 genes being involved in its assembly and DNA packaging (review: Black *et al.,* 1994). The wild-type capsid is a prolate icosahedron, ~850 Å wide by ~1150 Å long (Moody, 1999). Its caps conform to a triangulation number of T = 13 (Aebi *et al.,* 1974) and the elongated midsection to Q = 21 (Baschong *et al.,* 1988; Lane and Eiserling, 1990). The mature shell is made up of five proteins. There are nominally 960 subunits of the major capsid protein, gp23*; 55 copies of the minor capsid protein gp24*, occupying 11 of the 12 vertices; and a dodecamer of gp20 at the portal or connector vertex (Black *et al.,* 1994). In addition, 960 copies of Soc (small outer capsid protein) and 96–144 copies of Hoc (highly antigenic outer capsid protein) decorate the external surface (Baschong *et al.,* 1991).

Genetic studies combined with biochemical and structural analyses have led to a detailed account of morphogenesis (review: Kellenberger, 1990). The precursor proteins of the internal scaffold and the surrounding shell copolymerize out of an initiation complex containing gp20. On completion of the procapsid, the viral protease, gp21, is activated and processes all components except gp20 (Onorato and Showe, 1975). In particular, gp23 is converted to gp23* by removal of its N terminus, and gp24 is similarly truncated (see Black *et al.,* 1994). The cleaved procapsid undergoes a profound structural transformation, including a 15–20% expansion (Carrascosa, 1978; Steven *et al.,* 1976) that stabilizes this fragile particle and creates or exposes binding sites for Hoc and Soc.

The binding of accessory proteins to the outer surface of the capsid after it has matured from the procapsid state is widespread but not universal among dsDNA viruses. The binding of gpD to phage lambda (Sternberg and Weisberg, 1977) and of Soc to T4 (Ishii *et al.,* 1978; Steven *et al.,* 1992) significantly stabilizes the respective capsids. The roles of other accessory proteins, such as

[1] To whom reprint requests should be addressed at Bldg. 6, Rm B2-34, MSC 2717, National Institutes of Health, Bethesda, MD 20892-2717. Fax: (301) 402-7629. E-mail: Alasdair_Steven@nih.gov.

0042-6822/00 $35.00

T4 Hoc and VP26 of herpes simplex virus (Desai *et al.,* 1998), remain enigmatic. Since these proteins are at least conditionally dispensable, their binding may be decoupled from capsid assembly *per se*. This property has been exploited to develop them as fusion proteins that support the display of domains or protein subunits on the capsid surface at high copy number (Ren *et al.,* 1996; Jiang *et al.,* 1997).

Previous structural studies of T4, based on two-dimensional filtering of electron micrographs of tubular capsid analogs prepared by negative staining or shadowing, have revealed the hexagonal surface lattice of gp23/gp23* at successive stages of maturation, and the locations of Soc and Hoc (review: Black *et al.,* 1994). Cryo-electron microscopy combined with icosahedral image reconstruction allows more detailed analysis and has been applied to the capsids of several other phages (review: Baker *et al.,* 1999). Although the prolate form of T4 prevents straightforward application of these methods, there are at least two ways to circumvent this problem: (i) by basing the analysis on lower symmetry (Tao *et al.,* 1998) or (ii) by exploiting mutants that produce isometric capsids (Trus *et al.,* 1997; Tao *et al.,* 1998). Such T4 mutants have long been known: in particular, a set of "petite" (*pt*) point mutations that cluster in three loci in gene 23 (Eiserling *et al.,* 1970; Doermann *et al.,* 1973).

The goals of this study have been to investigate the structure of the T4 capsid with particular attention to the vertices and the binding properties of Soc and Hoc. First, to facilitate structural analysis, we optimized the yield of isometric capsids for one of the petite mutants. This mutant was combined with mutations in other genes, allowing us to isolate empty isometric capsids containing both Hoc and Soc or Hoc alone. Their structures were determined to resolutions of ~28 Å. In addition to depicting the three-dimensional structure of the T4 surface lattice, this analysis revealed that Soc has the unusual property of forming both monomers and trimers on the capsid surface. To examine the intrinsic propensity of Soc to oligomerize, we expressed the protein in *Escherichia coli* and investigated its oligomeric state in solution by analytic ultracentrifugation.

RESULTS

Populations of T4.pt21-34c Capsids with > 80% Isometrics

As a source of isometric capsids, we chose to work with the mutant *pt*21-34c (Doermann *et al.,* 1973; Mooney *et al.,* 1987). To avoid the potential complication to image analysis of densely packed, nonicosahedrally arranged DNA, we decided to use empty capsids and therefore crossed in a packaging-defective mutation in gene *17* (terminase large subunit—Rao and Black, 1988). To obtain capsids lacking Soc, a *Soc*-deletion mutant (MacDonald *et al.,* 1984) was crossed in, generating a *17am.23pt.soc-del* phage. The double mutant *17am.23pt*21-34c has not been described before, but we expected its morphological phenotype to be that of *23pt*21-34c, i.e., ~30% each of isometrics and normal prolate capsids and ~40% of intermediate-sized particles (Lane and Eiserling, 1990). However, in initial experiments, our yields of isometrics were <10%.

Petite mutant strains have a propensity to accumulate phage with normal-sized, prolate, capsids (Doermann *et al.,* 1973) since such revertants have a strong selective advantage over genotypes that produce isometric capsids, which accommodate only ~70% of the genome. Thus a cell must be infected with at least two isometric phages for the infection to be productive (most double infections should be productive, given the circularly permuted headful mode of DNA packaging employed by T4). To test this hypothesis for our low yields of isometrics, we started with single minute *17am.23pt*21-34c plaques and prepared low-titer stocks (~10^{10} phage/ml), restricting the number of amplification cycles to two. As determined by counting from cryo-electron micrographs (e.g., Fig. 1), ~81% of the capsids (N = 1652) produced by these stocks under nonpermissive conditions were isometric; the rest were of normal length, with few intermediates.

Protein composition

Hoc+.Soc+ and Hoc+.Soc− capsids were isolated by differential centrifugation followed by sucrose gradient centrifugation and "SDS cleaning," which eliminates unexpanded capsids and most contaminants (Steven *et al.,* 1976). Their purity was assessed by SDS–PAGE (Fig. 2a), and negative staining (data not shown) and cryo-electron microscopy (Fig. 1). The gel patterns showed the capsids to consist essentially of gp23*, gp24*, Hoc, and, if present, Soc (cf. lanes 5 and 6 of Fig. 2a). Gp20 was not detected in significant amounts and was probably dislodged by SDS cleaning. This inference is supported by cryo-micrographs, which show some particles with a peripheral patch of low density that may represent a vacant vertex (arrows, Fig. 1).

Gp24* is present in isometric capsids

One explanation for the altered head lengths of petite mutants is that they act as 24-bypass mutants (Johnson *et al.,* 1992). On the basis of the kinetic model, Showe and Onorato (1978) proposed that the mutant gp23 may bind to the vertices, bypassing the requirement for gp24. Since gp23 is abundantly expressed, the effective concentration of vertex protein would thus be enhanced, resulting in premature initiation of distal cap formation. However, *pt*21-34c was found not to exhibit the bypass phenotype (Lane and Eiserling, 1990). Nevertheless because the presence of gp24 in isometric capsids has not been demonstrated, we performed Western blotting with

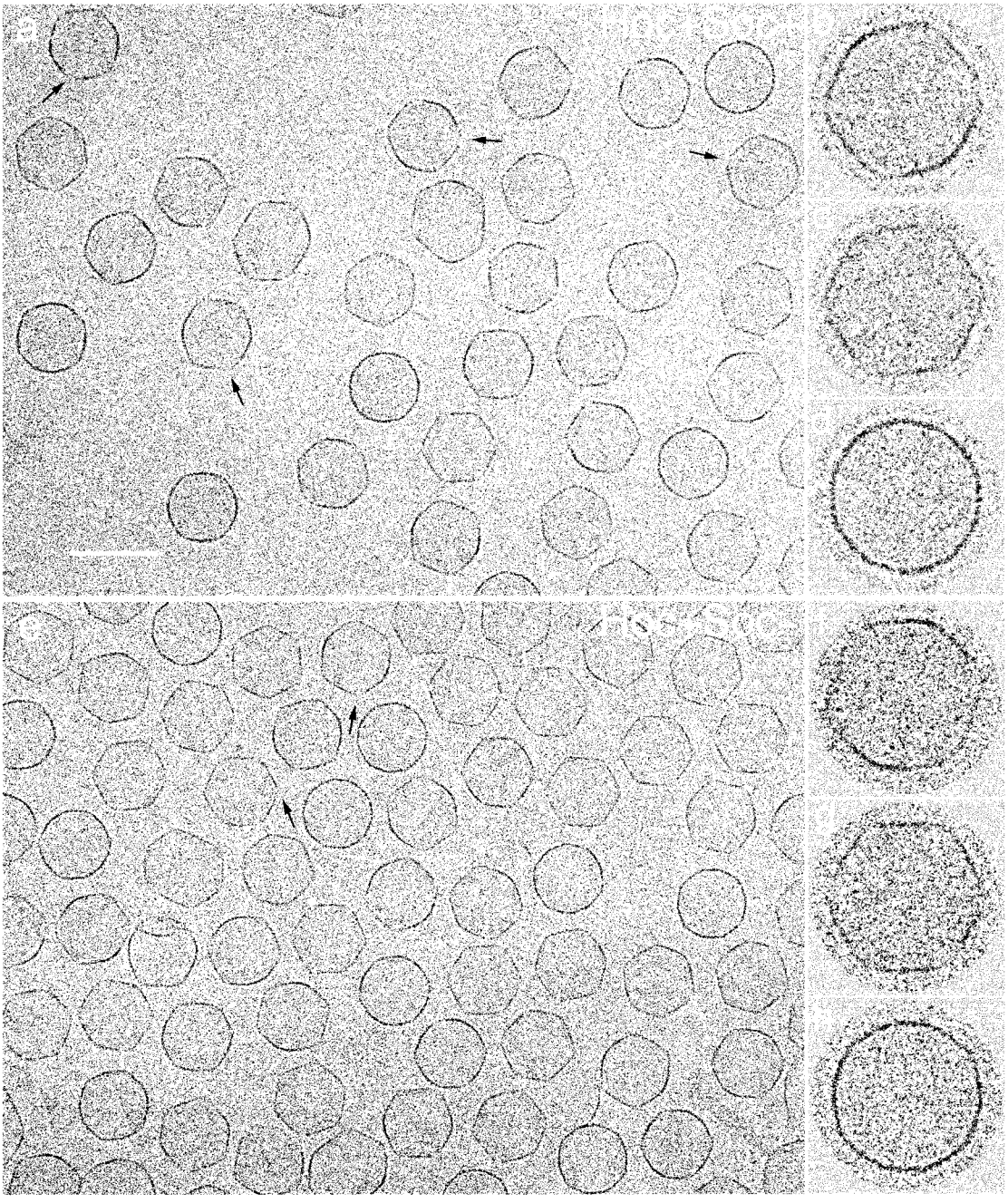

FIG. 1. Cryo-electron micrographs of (a–d) *17am.23pt*21-34c capsids, and (e–h) *17am.23pt*21-34c.*soc*− capsids. At right are shown, at higher magnification, particles viewed from directions close to twofold (b and f); threefold (c and g), and fivefold (d and h) axes of symmetry, respectively. Arrows in panels (a) and (e) denote particles that appear to have diminished density at a point on their periphery which correlates with loss of the connector/portal protein, gp20. Bar (a) = 1000 Å.

anti-gp24 antiserum (Fig. 2b). The data indicate that these capsids do indeed contain gp24*: in contrast, no gp24* was detected in bypass-24 capsids. Consistent with McNicol *et al.* (1977), we observed a doublet, presumably reflecting incomplete cleavage of gp24.

Capsid structure

Fields of Hoc+.Soc+ and Hoc+.Soc− capsids are shown in Fig. 1. The angular profiles projected by most of the capsids are indicative of relatively flat facets; particles that appear round are viewed along or close to a fivefold axis. Both kinds of capsids are notably thin-walled. In some views, peripheral serrations are faintly visible.

Three-dimensional density maps were calculated with resolutions of 29 Å (Hoc+.Soc+) and 27 Å (Hoc+.Soc−), respectively (Fig. 3). Both capsids exhibit the expected T = 13 *laevo* surface lattice. Their inner surfaces, which

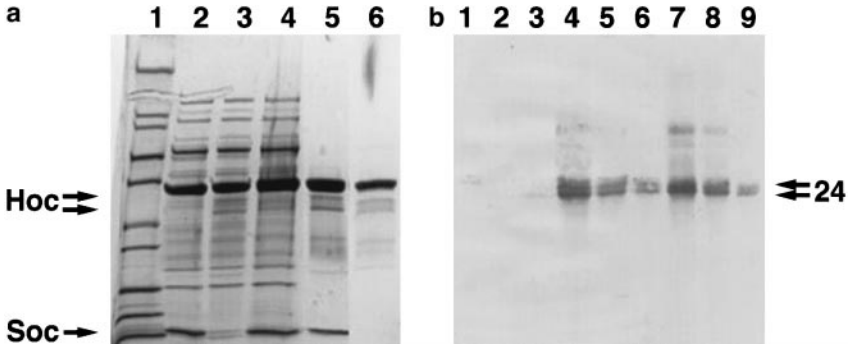

FIG. 2. (a) Protein composition of purified, predominantly isometric, T4 capsids. The proteins were separated by SDS–PAGE (Laemmli, 1970) on a 10–20% linear gradient gel and stained with Coomassie Blue (see Materials and Methods). Lane 5, purified Hoc+.Soc+ capsids; lane 6, Hoc+.Soc− capsids. The other lanes are as follows: lane 1, MW markers (Novex Mark 12); lane 2, Hoc−.Soc+ phage; lane 3, Hoc+.Soc− phage; lane 4, Hoc+.Soc+ phage. (b) Gp24 is present in isometric capsids. Purified isometric capsids (Hoc+.Soc−, lanes 7–9) or normal-length prolate capsids (lanes 4–6) or bypass24 phage (*24am*E303), purified by CsCl gradient centrifugation were subjected to SDS–PAGE on a 10% polycrylamide gel and gp24 was detected by blotting on to a nitrocellulose membrane (Towbin *et al.,* 1979) and immuno-staining with a polyclonal anti-gp24 antiserum kindly supplied by Dr L. Black, U. Maryland School of Medicine. The three lanes shown for each sample represent serial fivefold dilutions of samples that contained the same amount of gp23*, the major capsid protein. Note the absence of immunostaining in the byp24 sample (lanes 1–3). This mutant has an amber mutation in gene 24 (McNicol *et al.,* 1977) and the capsids lack gp24*. Another preparation of isometric *17am,23pt* capsids shared the same extent of staining as the *17am.23pt.soc*− capsids (lanes 7–9) (data not shown).

are indistinguishable, are smooth, consistent with prior observations of metal-shadowed polyheads (Kistler *et al.,* 1978). They show hexameric clusters of shallow protrusions, one per gp23* subunit, directly below the more pronounced protrusions on the outer surface. Also, the inner surface is visibly recessed beneath the pentons.

The outer surfaces are covered with complex patterns of protrusions (Figs. 3a, 3c, and 4). These patterns confirm the conclusions of earlier negative staining studies of the hexagonal (i.e., non-vertex) portions of the respective surface lattices. In both cases, rings of six protrusions, each ~24 Å long by 23Å wide, rise 15Å above a thin sheet of density that appears continuous at the current resolution. In particular, no holes are seen. The centers of these protrusions, each associated with a gp23* monomer, lie at a radius of ~42 Å from the center of each hexamer regardless of whether or not Soc is present.

The most notable feature of the vertex capsomer is a ring of five protrusions on the outer surface, each presumably contributed by a gp24* subunit. These protrusions are similar in size and positioning relative to the center of the capsomer to those of gp23* hexamers.

Binding of Hoc

The largest protrusion, at the center of the gp23* rings, represents an averaged Hoc monomer. Clearly, Hoc is absent from the gp24* pentamer (Figs. 3 and 4). The Hoc-associated protrusion is more prominent in the Hoc+.Soc− density map, possibly reflecting more complete occupancy in this preparation of capsids. (These preparations derive from *17am* mutants and contain expanded capsids both with the available accessory proteins and without. The latter represent particles that were cleaved but not expanded at the time of cell lysis (Carrascosa, 1978). The relative amounts of the two kinds of capsids vary somewhat from preparation to preparation (Steven *et al.,* 1992).

As visualized, the Hoc protrusion is smaller than we would expect for a 40-kDa protein. Although the division between Hoc and the underlying gp23* lattice can only be defined conclusively when a Hoc− reconstruction is obtained, we currently estimate this protrusion to have a volume corresponding to 10–15 kDa of protein. The reasons for this discrepancy are not evident: it may represent partial occupancy; the volume common to subunits in different symmetry-related sites; or that the Hoc molecule is partly disordered, e.g., as a result of SDS cleaning.

Binding of Soc

At the trigonal points where three gp23* hexamers meet are triplet protrusions contributed by Soc trimers. The subunits are elongated (~39 Å long by 27 Å wide), giving the trimer the appearance of a propellor whose blades are set at a small angle (~5°) relative to the lines between lattice points. Their volume is appropriate for a 9-kDa subunit.

Interestingly, around the trigonal points adjacent to the vertices, where two gp23* hexamers and one gp24* pentamer meet, there is only one Soc subunit. Since two gp23*-gp24* interfaces and one gp23*-gp23* interface cluster around this point, it follows that if either of the paired subunits is gp24* instead of gp23*, the binding is not strong enough to secure a Soc subunit. Thus prolate capsids (Q = 21) with a full complement of accessory proteins should have 840 copies of Soc—fewer than the previous figure of 960—and 160 copies of Hoc. Similarly, isometric capsids should have 660 copies of Soc and 120 copies of Hoc.

The interaction of Soc with the underlying gp23* sur-

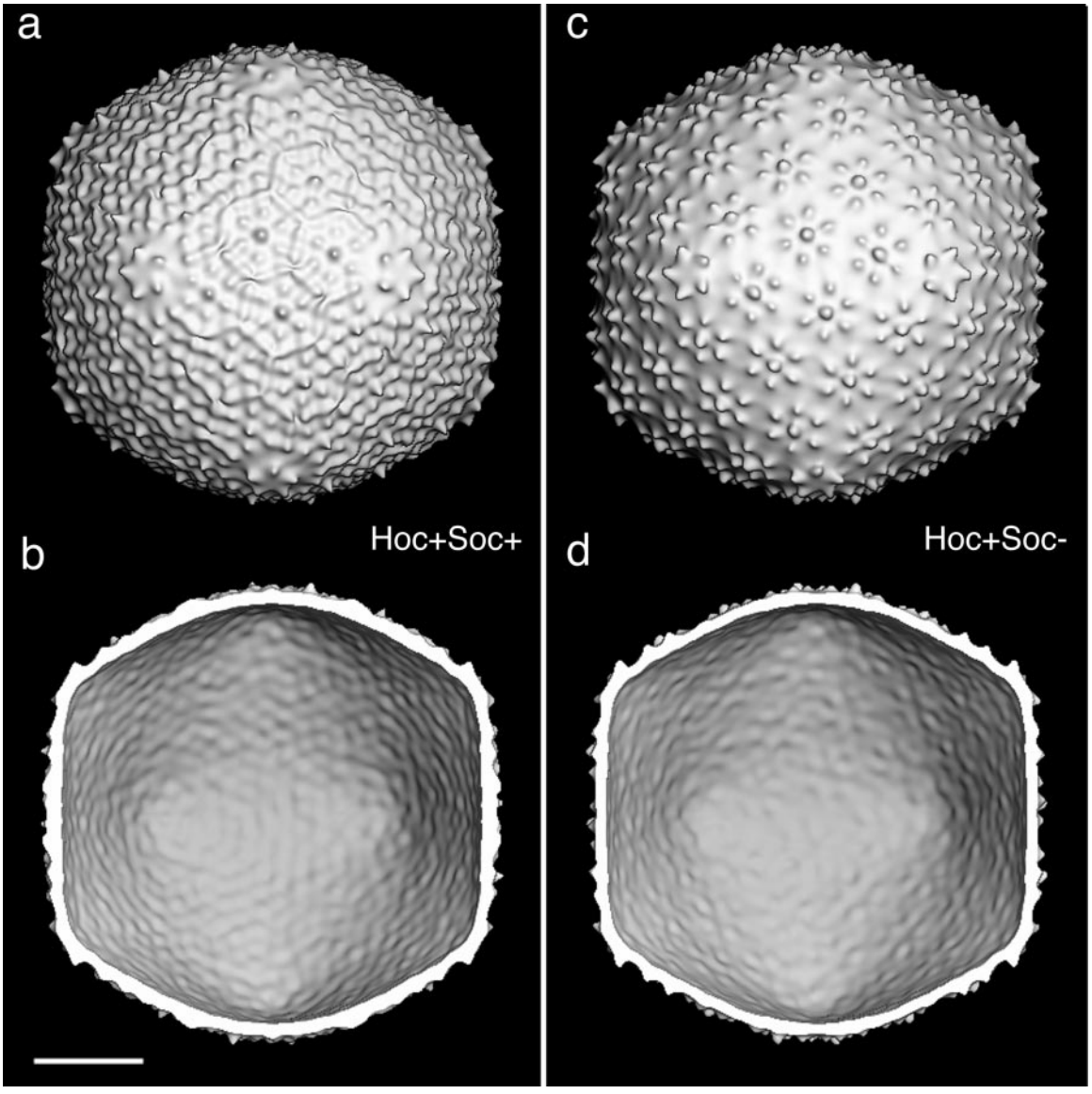

FIG. 3. Structures of isometric T4 capsids, Hoc+.Soc+ (a and b) and Hoc+.Soc− (c and d), as viewed along axes of twofold symmetry. (a and c), outer surfaces; (b and d), inner surfaces. Bar = 200 Å.

face lattice was studied further by comparing serial sections tangential to the capsid surface for both the Soc+ and the Soc− particles (Fig. 5). Although our maps do not delineate the boundaries between capsomers, they show that Soc is centrally placed between adjacent hexamers, straddling the lattice line that runs between them, connecting two local threefold axes. This observation suggests that each Soc subunit interacts with two gp23* subunits, bridging the interface between them. These sections also show that the subunits in Soc trimers come closest together at a level that is above, not directly on, the gp23* surface lattice (Fig. 5).

Soc is a monomer in solution

Capsid-bound Soc is monomeric at the trigonal sites closest to the vertices and trimeric elsewhere (Fig. 4a). This duality raises the question: what are its intrinsic oligomerization properties? To address it, we cloned Soc under the control of a phage T7 promoter, expressed it in *E. coli*, and purified the resulting protein (Fig. 6). Soc refolds readily after being exposed to denaturants, and this property facilitated its isolation. Soc prepared in this manner is competent to bind to polyheads (Ren *et al.,* 1996). That it is folded was further attested by circular dichroism measurements (Fig. 7a), which yielded a spectrum typical of a protein with a substantial content of β structure. Deconvolution of this spectrum yielded estimates of ~10% α-helix and 50–60% β sheet (Table 1).

It was our experience that Soc exhibits limited solubility *in vitro*, up to a limit of ~5 mg/ml. In measuring its state of aggregation by analytical ultracentrifugation, we used initial protein concentrations of 0.1–1.0 mg/ml, well

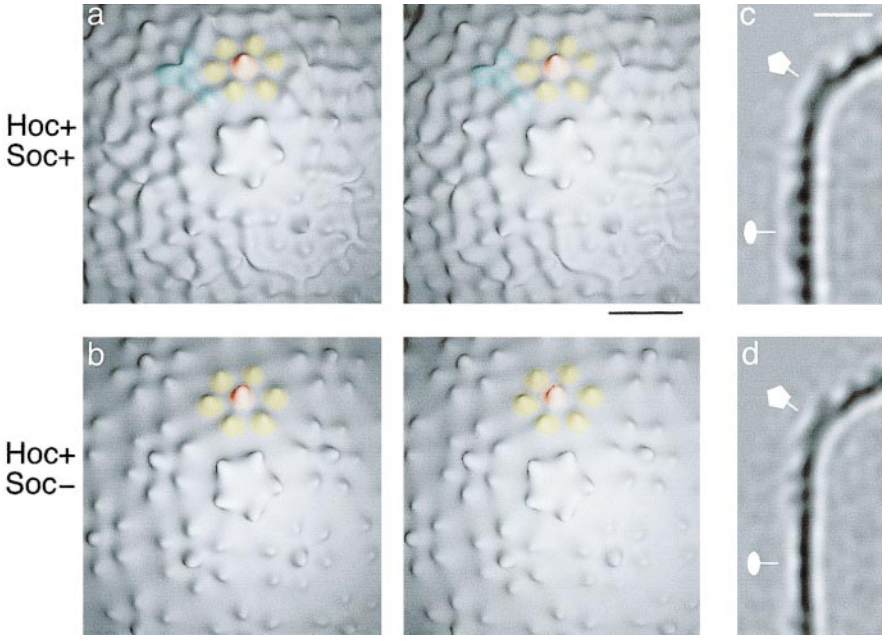

FIG. 4. Stereo pairs representing the vertices and surrounding areas on the outer surfaces of T4 isometric capsids: (a) Hoc+.Soc+ and (b) Hoc+.Soc−. The six gp23*-associated protrusions on one hexamer are tinged gold (each protrusion represents a 5–6 kDa outcrop of the 49-kDa subunit); the single Hoc-associated protrusion at the hexamer center is tinged red; and Soc-associated protrusions are tinged turquoise for one monomer and one trimer. Bar = 100 Å. (c) and (d) show portions of central sections through the respective density maps as viewed along twofold axes. The positions of five- and twofold symmetry axes are marked. The sections reveal the thinness (~30 Å) of the capsid walls, the low relief of their surface features, particularly on the inner surface, and the absence of holes of any significant size. Bar = 100 Å.

below this limit. A typical equilibrium curve is shown in Fig. 7b (the starting concentration was 0.25 mg/ml). Analysis of these data yielded a molecular weight of 9000, i.e., a monomer, with no indication of higher oligomers.

DISCUSSION

A molecular mosaic

The architectural principle of modulating the properties of a protein polymer by binding additional proteins at strategic sites is widespread in biology—among cytoskeletal filaments, for example (review: Fuchs and Yang, 1999). The T4 capsid affords a valuable model system of this kind for the study of protein–protein interactions and biopolymer design. Its basic matrix is a hexagonal net of gp23* hexamers folded into a closed icosahedral shell. Inserted in this net at sites of local fivefold symmetry are pentamers of gp24*and a dodecamer of gp20, the latter forming a specific pore through which DNA and proteins may pass (Mullaney and Black, 1998). Bound to the surface lattice around sites of local threefold symmetry are molecules of Soc that contribute structural reinforcement and, at sites of local sixfold symmetry, monomers of Hoc. The potentiality of the T4 capsid for display of domains and proteins on Soc and Hoc and for "biopolymer engineering" provides an incentive for seeking a better understanding of its basic properties.

Production of *pt*21-34 isometric capsids

By restricting propagation to two cycles, starting from single petite plaques, we obtained capsid preparations with 80% of isometrics. However, this percentage dropped on further propagation, supporting the view that isometric T4 phages rapidly accumulate revertants and pseudorevertants because the requirement for multiple coinfection puts them at a competitive disadvantage relative to phages with normal-sized capsids (Haynes and Eiserling, 1996). It seems unlikely that the isometric phenotype can be stably maintained unless a viable genome of ~70% of wild-type size could be constructed by eliminating dispensable functions, thus relieving the pressure to revert. However, such an undertaking would be evolutionarily regressive in the sense that it appears likely that the prolate capsid morphology and specialized vertex protein of T-even phages were selected specifically to accommodate larger genomes (i.e., ones encoding additional functions).

Our data imply that *pt*21-34c preferentially assembles isometric capsids rather than intermediate-sized capsids. It may be that capsids of the latter kind result from coexpression of *pt*21-34c and revertant *g*23 in appropriate ratios. In this scenario, the distribution of variously sized particles obtained under given experimental conditions reflects the prevalent ratio of the two kinds of gp23, i.e., the state of reversion in the phage stock. The

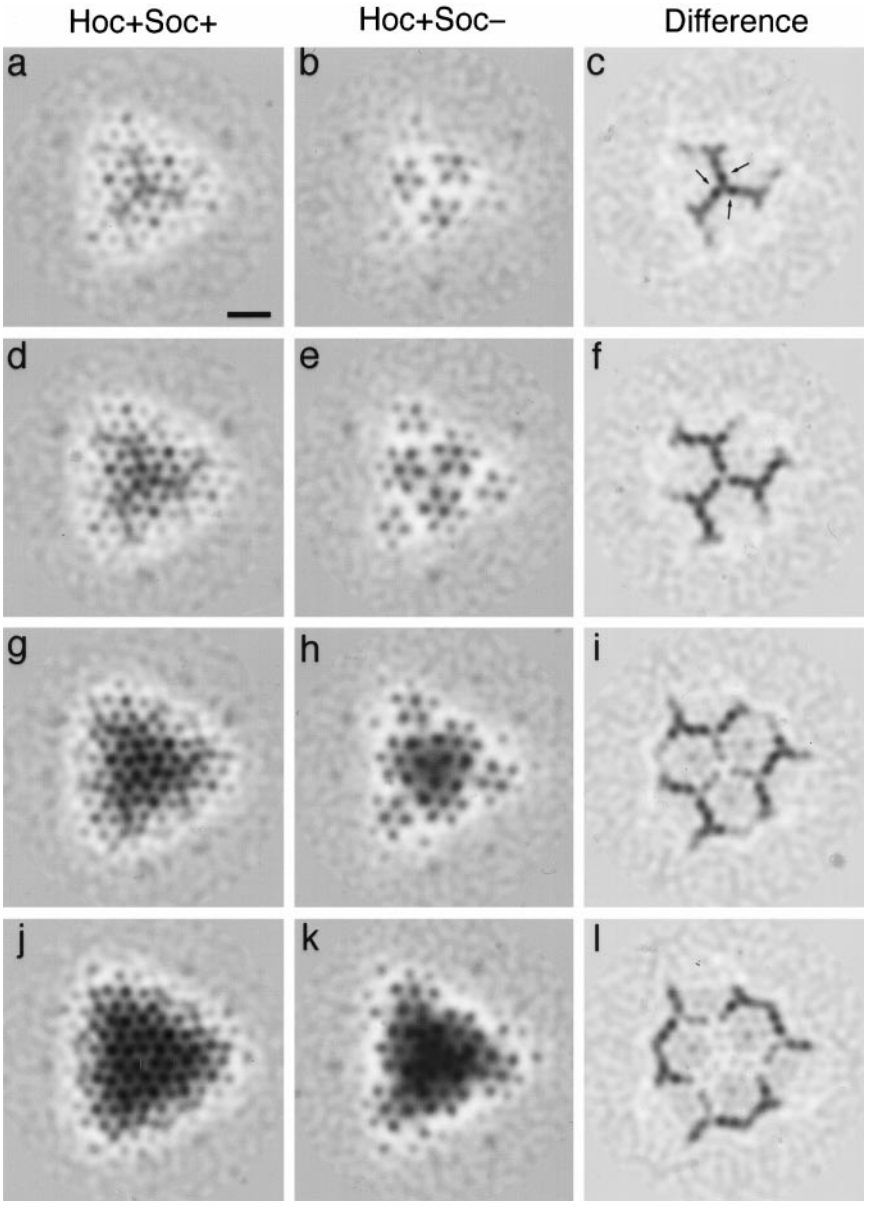

FIG. 5. Serial sections through the density maps of the Hoc+.Soc+ (left) and Hoc+.Soc− (center) isometric T4 capsids and the difference map between them (right). The sections, centered on a threefold axis of symmetry, are parallel to the capsid surface and are 2.3 Å thick and spaced 7.3 Å apart. The difference map shows the Soc molecules. In the first row (a–c), the section passes centrally through the Soc trimer at the icosahedral threefold axis, whose three subunits are marked with small arrows in (c). In the next section, (f), these three subunits do not make contact. Bar (a) = 100 Å.

plaques produced by *17am.23pt*21-34c tend to be smaller than wild type and heterogeneous in size. The latter property may reflect the timing at which revertants and/or pseudorevertants happen to arise during the formation of a given plaque.

Topology of a molecular clamp

Visualization of single Soc molecules at the peripentonal sites (Fig. 4a) allows us to equate each blade of the trimeric propellor with a separate Soc subunit. Subject to the *caveat* of limited resolution, the three Soc subunits appear to make contact at the center of the propellor (Figs. 5c and 5i). However, this interaction is insufficient for trimer formation as both the ultracentrifugation data and the visualization of Soc monomers attest. Instead trimerization of Soc appears to be imposed by a template of three suitably spaced binding sites on the gp23* surface lattice. A similar situation occurs with gpD, Soc's counterpart in phage lambda: gpD is a monomer in solution (Imber *et al.,* 1980) but forms a trimer on the capsid (Yang *et al.,* 2000). However, the two proteins differ in that gpD forms a closely annealed trimeric ring

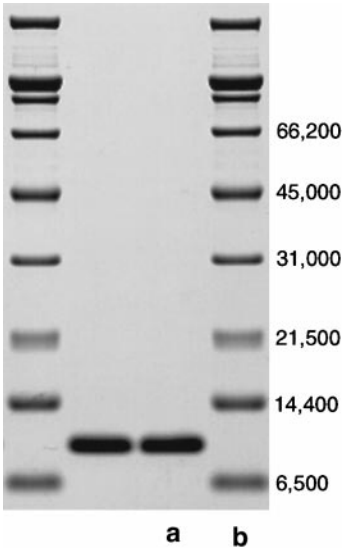

FIG. 6. Bacterially expressed and purified Soc protein, characterized by SDS–PAGE with Coomassie Blue staining. Duplicate samples are shown of Soc (a) with MW markers in the outside lanes (b).

and has little regular secondary structure (Yang *et al.,* 2000) in contrast with Soc's predominant β-structure.

Comparison of the Soc+ and Soc− reconstructions suggests that each Soc subunit interacts with two gp23* capsomers (Fig. 5), thus serving as an intermolecular clamp (Steven *et al.,* 1992). Thus the mechanism whereby Soc stabilizes the capsid, increasing its thermal denaturation temperature by 6°C (Ross *et al.,* 1985) and its resistance to alkaline pH (Ishii and Yanagida, 1977), appears to reflect a set of cooperative interactions. Soc subunits bridge the intercapsomer interfaces, with possible reinforcement by secondary Soc–Soc interactions at the center of the trimer.

Vertex structure: comparative properties of gp24* and gp23*

The assignment of gp24* to the 11 nonportal vertices was based on the observation of holes in capsids after treatment with urea, which extracted gp24* (Müller-Salamin *et al.,* 1977). That gp24* should form pentamers is consistent with biochemical estimates of copy numbers (62–67 for mature heads; 59–88 for proheads—Onorato *et al.,* 1978; Baschong *et al.,* 1991), allowing a reasonable margin of error. However, this has not been demonstrated directly and was not a foregone conclusion since symmetry mismatches are not unusual at capsid vertices (e.g., trimeric fibers are found at adenovirus vertices). Our observation of pentons with sharply expressed fivefold symmetry affords quite strong evidence that they are indeed pentamers. If they were some other oligomer, imposition of fivefold symmetry in the reconstruction would have resulted in a cylindrically symmetric appearance or, at most, weakly contrasted fivefold symmetry.

Gp24* and gp23* share only limited sequence similarity. (The gp24 sequence—Accession No. P19896—was deposited in the database by K. Yasuda and colleagues in 1996). We detected only 24% identity after aligning the two proteins by a BLAST search (Altschul *et al.,* 1990). The terminal regions of the respective precursor proteins show no sequence similarity and the δ region that is removed by proteolysis appears to be much smaller for gp24, i.e., 10 residues, compared with 65 for gp23. The predicted sizes of the mature proteins are 417 residues (gp24*) and 456 residues (gp23*). Since the cryo-EM maps show the gp24* pentamer to be very like a fivefold version of the gp23* hexamer, it follows that the respective subunits should also be similar in shape. Thus they may well have similar folds, but differ in their propensity to oligomerize (van Driel, 1980).

Osmotic shock resistance

Another distinction between gp24* and gp23* is that gp24* binds neither Soc nor Hoc. It was previously observed that the various quasiequivalent Soc binding sites on the hexagonal lattice of giant Soc− capsids have differing affinities, reflecting differences in local curvature of the gp23* surface lattice (Aebi *et al.,* 1977). However, these distinctions differ from the all-or-nothing effect that we observe on isometric capsids whereby all Soc binding sites on the gp23* lattice are fully occupied, and all of the corresponding sites in which gp24* is involved are completely unoccupied.

The failure of gp24* to bind Soc provides a possible explanation for the property of osmotic shock resistance, which was mapped to gene 24, while no accompanying alteration was seen in the hexagonal surface lattice of Os-shock resistant giant phage capsids (Leibo *et al.,* 1979). A likely mechanism is that the capsid may rupture at a gp24*-containing vertex when subjected to osmotic stress. With reference to the "molecular clamp" role played by Soc (see above), it may be that its absence from interfaces in which gp24* is involved accounts for the observed weakness, and that Os-resistant mutant gp24* has acquired the ability to bind Soc, thus stabilizing the capsid. Alternatively, these mutations could affect residues located at interfaces with gp23* or other gp24* subunits, resulting in a stronger interaction and enhanced resistance to osmotic stress.

Implications for phage display on Soc and Hoc

Both Soc and Hoc have the capacity to display whole domains and proteins (Ren *et al.,* 1996; Jiang *et al.,* 1997; Ren and Black, 1998). Display may be effected either *in vivo* by incorporating an appropriate Soc or Hoc fusion in the T4 genome or *in vitro* by expressing the fusion protein and then binding it to isolated capsids or related

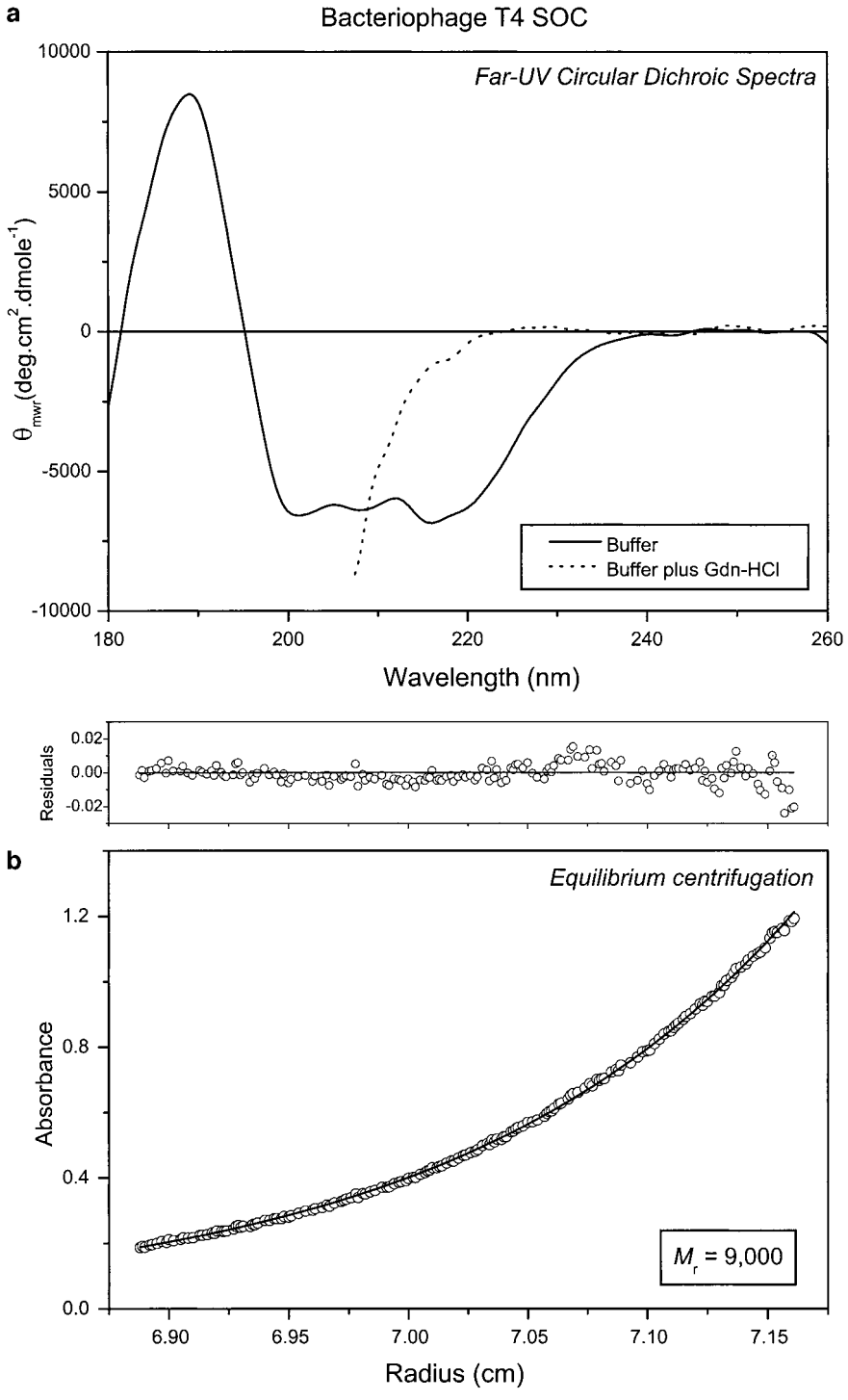

FIG. 7. (a) shows the far-UV circular dichroic spectra of Soc in buffer alone and in the presence of 4 M guanidine–HCl. The loss of secondary structure in the presence of the denaturant affirms the native-like conformation of the protein. The secondary structure calculations listed in Table 1 are from the native spectrum. (b) shows the absorbance gradient (protein concentration range ~0.05–1.0 mg/ml) in the analytical centrifuge cell after attaining sedimentation equilibrium at 30,000 rpm. The open circles are the experimental data, and the solid line is the result of fitting to a single ideal species. The corresponding upper panel shows the residuals between the fitted and experimental values as a function of radial position. The molecular weight determined from the data are 9000 and this compares with 8986 calculated from the predicted protein sequence, indicating that Soc is a monomer in solution.

particles. The practicability of this approach is supported by the readiness with which Soc appears to refold after exposure to denaturing conditions.

One prospective application of this technology—structural analysis of the displayed moiety by cryo-EM (Ren *et al.,* 1996)—is applicable to proteins or complexes

TABLE 1

Secondary Structure of Soc (%) Calculated from Circular Dichroic Spectra

Method[a]	α-Helix	β sheet	β turn	Other
A	13	36	25	26
B	5	26	21	49
C	6	58	0	36

[a] A, B and C refer to the methods of Sreerama and Woody (1993), Perczel *et al.* (1992), and Chang *et al.* (1978), respectively.

whose limited solubility makes them refractory to X-ray crystallography or NMR spectroscopy. Here the T4 system offers two options: helical reconstructions, using polyheads as the display platform, or icosahedral reconstructions of isometric capsids. In this context, Hoc and vertex-proximal Soc appear to be particularly well suited for the display of large complexes in view of their exposed positions and ample surrounding space (Fig. 4a).

MATERIALS AND METHODS

Bacteria, phage, and construction of mutants

E. coli P301(Su−) was used as the nonsuppressor strain and B40(Sul+) as the suppressor strain for amber mutants. Luria Bertani-Miller medium (LB) was used for most of the *E. coli* and phage culturing and plating experiments. M9S medium was used for preparation of large phage stocks. A 50:50 mixture of LB and M9S was used for phage mutant infections in the capsid isolation experiments. The media are described by Maniatis *et al.* (1982).

Wild-type T4 and the mutant *17*amNG178 were from laboratory stocks. The *Soc*- deletion mutant (MacDonald *et al.,* 1984) was kindly provided by Dr G. Mosig (Vanderbilt), *23pt*21-34c by Dr. F. Eiserling (UCLA), and *24am*E303.byp24 by Dr L. Black (U. Maryland). In the latter mutant Ala-275 is altered to Thr (Mooney *et al.,* 1987). The mutants *23pt*21-34c.*17am*NG178, and *23pt*21-34c.*17am*NG178.*soc*− were constructed by standard genetic crosses. Since *23pt*21-34c shows a small plaque phenotype, such progeny plaques were first selected and then screened for the second mutant used in the cross. Once potential recombinants were identified and plaque-purified, each mutant stock was checked for isometric phages by EM, to confirm the presence of the *23*pt21-34c mutation. The presence of the *soc*− deletion in recombinants was assayed by screening a large number of single-plaque stocks for sensitivity to pH 10.6 (Ishii and Yanagida, 1977). The absence of Soc was confirmed by SDS–PAGE of phage particles.

Preparation of stocks of petite mutants

Because revertants accumulate rapidly during serial subculturing of petite mutants, the following protocol was used. A minute plaque was picked and resuspended in 500 μl of phosphate buffer containing several drops of chloroform. After incubation at room temperature for several hours with intermittent vortexing, the whole lysate was used to infect *E. coli* B40 and plated on LB agar. After overnight incubation, the top layer was scraped off into 100 ml of exponentially growing culture at $\sim 1 \times 10^8$ cells/ml, ensuring that all cells were productively infected at 1 m.o.i. The infected culture was incubated with shaking at 37°C for 1–2 h, then 10 ml of chloroform was added, and shaking was continued for 10 min. The lysate was centrifuged at 15,000 rpm for 45 min, the supernatant discarded, and the pellet resuspended in 15 ml of phosphate buffer containing 10 μg/ml of pancreatic DNase I and several drops of chloroform. The lysate was then incubated at 37°C for 30–60 min with occasional shaking and was centrifuged at 7000 rpm for 12 min. The supernatant containing the phage was stored at 4°C. The titers, typically $1–3 \times 10^{10}$ phage per ml, were suitable for preparation of isometric capsids. When additional stocks were needed, the procedure was repeated, starting with a single plaque, as described above.

Preparation of capsids

E. coli P301 was grown on LB-M9S medium (100 ml) at 37°C to a density of 4×10^8 cells/ml and infected with *23pt*21-34c.*17am*NG178 (Hoc+ Soc+) or *23pt*21-34c.*17am*NG178.*soc*- (Hoc+ Soc−) at a multiplicity of 2.5–5.0, then superinfected at the same multiplicity 7 min later. Thirty minutes after infection, the culture was centrifuged at 7000 rpm for 12 min, and the pellet was resuspended in 5 ml of Buffer I (50 mM Tris–HCl, pH 7.4, 5 mM $MgCl_2$, 3 mM β-mercaptoethanol) plus 10 μg/ml DNAase I and ~20 drops of chloroform. The sample was incubated at 37°C for 20–30 min with occasional shaking, then was diluted with 20 ml of Buffer II (Buffer I with 50 mM NaCl) and was centrifuged at 7000 rpm for 12 min. The supernatant was centrifuged at 18,000 rpm for 45 min to pellet the capsids. The pellet was resuspended in 1 ml of Buffer II, and 10% SDS was added to a final concentration of 1%. The samples were incubated at 37°C for 20 min, then were diluted with 12 ml of Buffer II, and were subjected to two rounds of low- and high-speed centrifugation as described above to remove SDS. The final pellet was resuspended in 100 μl of Buffer II, loaded onto a 14-ml 5–45% linear sucrose gradient in Buffer II, and spun at 40,000 rpm for 2.5 h at 4°C in a Beckman 40Ti rotor. A sharp band of capsids was visible ~2.5 cm from the bottom of the tube. At least one additional band is seen slightly above the major band. The major band was extracted from the side of the tube with a syringe and dialyzed against 1000 ml of Buffer II overnight at 4°C. The dialysis was continued for 4–6 h with one change of buffer. The sample was then pelleted by

centrifuging at 18,000 rpm for 45 min and resuspended in 40 μl of Buffer II.

Cryo-electron microscopy and image processing

Drops (3.5 μl) of capsid suspensions were applied to the carbon side of holey carbon support films. Excess solution was blotted off and the specimen was plunged into liquid ethane slush, embedding it in vitreous ice. Grids were examined on a CM120 electron microscope (FEI, Mahwah, NJ) operating at 120 kV, with LaB_6 illumination. Electron micrographs were recorded at a nominal magnification of ×35,000 on Kodak SO-163, using minimal dose procedures, corresponding to ~10 electrons/Å^2 per exposure.

The isometric Hoc+.Soc− capsid was reconstructed from a focal pair of micrographs whose first contrast transfer function (CTF) zeros were at 17.8 and 22.5 Å, respectively. They were scanned on a Perkin–Elmer 1010MG microdensitometer, using 17-μm pixels (4.9 Å at the specimen). Image pairs (434) were picked with X3D (Conway *et al.,* 1993). Initial estimates of orientations and origins were obtained by applying the Polar Fourier Transform algorithm (Baker and Cheng, 1996) to the further-from-focus images, using a reference model produced by MODEL (Trus *et al.,* 1996). This program generates capsids of specified T numbers, with subunits represented as spherical balls. For our starting T = 13 model, the sizes of the subunits and their positions in the unit cell were assigned from prior negative staining work (cf. Fig. 10 of Black *et al.,* 1994). Hoc was assigned to the centers of both hexons and pentons. After this step, a density map was calculated and exhaustively refined by PFT. Then the closer-to-focus images were merged in, using the CTFMIX program (Conway and Steven, 1999), and the combined data were further refined. The final map included 162 image pairs and has 28.5 Å resolution (FSC = 0.3, Saxton and Baumeister, 1982). The surface renderings shown are contoured to enclose 100% of expected mass.

The Hoc+.Soc+ isometric capsid was reconstructed in similar fashion. Two focal pairs with first CTF zeros at (22.8 and 27.7Å) and (20.and 26.7Å), respectively, plus a single micrograph (CTF zero, 24.3Å) yielded 613 capsid images, of which 366 were independent. These data were processed as described above, using the Hoc+.Soc− density map as starting model. However, most of the near-threefold views turned out to be incorrectly assigned as twofold views, and a high incidence of other incorrect solutions occurred, as diagnosed by comparing model reprojections with original images. These problems persisted despite optimizing the scaling of the model to the data, and trying alternative, MODEL-generated starting models. Eventually, they were resolved by starting the PFT search at very low resolution (bandwidth: 400 to 100 Å) and gradually extending to an outer limit of 25–30Å. The final density map, calculated from 257 independent images (i.e., combined focal pairs or single images) had a resolution of 29 Å (FSC cutoff = 0.3).

To counter the concern that the final reconstructions might simply reproduce the starting model, we note that (i) the Hoc originally modeled at the center of the penton and the Soc at the peripentonal sites both disappeared and (ii) the correlation coefficients eventually obtained at 30 Å resolution are significantly higher than those that we obtained in analyses that ended inconclusively, i.e., without an evident T number or a consistent pattern of capsomer features.

Expression and purification of Soc

Soc was expressed in *E. coli* HMS174 (DE3) containing the plasmid pE-SOC I as described by Ren *et al.* (1996). The insoluble fraction containing Soc was solubilized in 4 M guanidine–HCl, was purified by gel filtration, and was folded by a simple dialysis scheme with a recovery of 90%. N-terminal sequencing confirmed the identity of residues 1–20; the initiating Met was completely processed. The concentration of purified Soc was determined by UV absorbence (Wetlaufer, 1962). The 79-residue protein (MW = 8986, from the DNA sequence) had a calculated molar extinction of 18mM^{-1} ($A_{0.1\%}$ = 2.00) at 280 nm with a 1-cm path length cell.

As an alternative to bacterial expression, Soc may be recovered from purified capsids by boiling them for 5 min in PBS buffer and then cooling. Soc remains in solution, apparently refolded, as judged by its ability to bind to capsids, whereas the other capsid proteins, having been thermally denatured, settle out as a flocculent precipitate (E. G. Locke and A.C.S.—unpublished results).

Circular dichroism and analytical ultracentrifugation

Measurements were made on a Jasco J720 spectropolarimeter using 0.01-cm path length cells (Hellma) and a 1-nm bandwidth. The protein (0.5 mg/ml) in 50 mM sodium phosphate, pH 7.2, was filtered and was degassed prior to analysis. The predicted monomer mass—8986 Da—was used to calculate mean residue ellipticities, which were used in calculating secondary structure from the CD spectra.

The molecular weight of Soc was determined by equilibrium centrifugation at 30,000 rpm for 17 h at 20°C on a Beckman XLA Optima analytical ultracentrifuge with an An-60 Ti rotor and standard double sector centerpiece cells. The buffer was 50 mM sodium phosphate, pH 7.2, with 0.15M NaCl. Solvent density was calculated according to Laue *et al.* (1992). The partial specific volume of Soc (0.73) was calculated from the predicted amino acid composition (Cohn and Edsall, 1943). Centrifugation data were analyzed using the Beckman-Origin software (v2.0 for Windows).

ACKNOWLEDGMENTS

We thank Jean Wang for developing the initial version of MODEL, Aimée Crago for carrying out the solubility trials with guidance from Adam Zlotnick, David Belnap for sharing unpublished results, and James Conway and Tim Baker for software. This project was initiated during V.R.'s sabbatical in the LSBR.

REFERENCES

Aebi, U., Bijlenga, R., v d Broek, J., v d Broek, H., Eiserling, F., Kellenberger, C., Kellenberger, E., Mesyanzhinov, V., Müller, L., Showe, M., Smith, R., and Steven, A. (1974). The transformation of tau particles into T4 heads. II. Transformations of the surface lattice and related observations on form determination. *J. Supramol. Struct.* **2,** 253–275.

Aebi, U., van Driel, R., Bijlenga, R. K., ten Heggeler, B., van den Broek, R., Steven, A. C., and Smith, P. R. (1977)., Capsid fine structure of T-even bacteriophages. Binding and localization of two dispensable capsid proteins into the P23* surface lattice. *J. Mol. Biol.* **110,** 687–698.

Altschul, S. F., Gish, W., Miller, W., Myers, E. W., and Lipman, D. J. (1990). Basic local alignment search tool. *J. Mol. Biol.* **215,** 403–410.

Baker, T. S., and Cheng, R. H. (1996). A model-based approach for determining orientations of biological macromolecules imaged by cryoelectron microscopy. *J. Struct. Biol.* **116,** 120–130.

Baker, T. S. Olson, N. H., and Fuller, S. D. (1999). Adding the third dimension to virus life cycles: Three-dimensional reconstruction of icosahedral viruses from cryo-electron micrographs. *Microbiol. Mol. Biol. Rev.* **63,** 862–922.

Baschong, W. C., Aebi, U., Baschong-Prescianotto, C., Dubochet, J., Landmann, L., Kellenberger, E., and Wurtz, M. (1988). Head structure of bacteriophages T2 and T4. *J. Ultrastruct. Mol. Struct. Res.* **99,** 189–202.

Baschong, W., Baschong-Prescianotto, C., Engel, A., Kellenberger, E., Lustig, A., Reichelt, R., Zulauf, M., and Aebi, U. (1991). Mass analysis of bacteriophage T4 proheads and mature heads by scanning transmission electron microscopy and hydrodynamic measurements. *J. Struct. Biol.* **106,** 93–101.

Black, L. W., Showe, M. K., and Steven, A. C. (1994). Morphogenesis of the T4 head. *In*: "Molecular Biology of Bacteriophage T4" (J. Karam, Ed.), pp. 218–258. Am. Soc. Microbiol., Washington, DC.

Carrascosa, J. L. (1978). Head maturation pathway of bacteriophages T4 and T2. IV. In vitro transformation of T4 head-related particles produced by mutants in gene 17 to capsid-like structures. *J. Virol.* **26,** 420–428.

Chang, C. T., Wu, C.-S., and Yang, J. T. (1978). Circular dichroic analysis of protein conformation: Inclusion of the beta-turns. *Anal. Biochem.* **91,** 13–31.

Cohn, E. J., and Edsall, J. T. (1943). "Proteins, amino acids and peptides." Van Nostrand-Reinhold, Princeton, NJ.

Conway, J. F., and Steven, A. C. (1999). Methods for reconstructing density maps of "single" particles from cryoelectron micrographs to subnanometer resolution. *J. Struct. Biol.* **128,** 106–118.

Conway, J. F., Trus, B. L., Booy, F. P., Newcomb, W. W., Brown, J. C., and Steven, A. C. (1993). The effects of radiation damage on the structure of frozen hydrated HSV-1 capsids. *J. Struct. Biol.* **111,** 222–233.

Desai, P., DeLuca, N. A., and Person, S. (1998). Herpes simplex virus type 1 VP26 is not essential for replication in cell culture but influences production of infectious virus in the nervous system of infected mice. *Virology* **247,** 115–124.

Doermann, A. H., Eiserling, F. A., and Boehner, L. (1973). Genetic control of capsid length in bacteriophage T4. I. Isolation and preliminary description of four new mutants. *J. Virol.* **12,** 374–385.

Eiserling, F. A., Geiduschek, E. P., Epstein, R. H., and Metter, J. (1970). Capsid size and deoxyribonucleic acid length:the petite variant of bacteriophage T4. *J. Virol.* **6,** 865–876.

Fuchs, E., and Yang, Y. (1999). Crossroads on cytoskeletal highways. *Cell* **98,** 547–550.

Haynes, J. A., and Eiserling, F. A. (1996). Modulation of bacteriophage T4 capsid size. *Virology* **221,** 67–77.

Imber, R., Tsugita, A., Wurtz, M., and Hohn, T. (1980). Outer surface protein of bacteriophage lambda. *J. Mol. Biol.* **139,** 277–295.

Ishii, T., Yamaguchi, Y., and Yanagida, M. (1978). Binding of the structural protein Soc to the head shell of bacteriophage T4. *J. Mol. Biol.* **120,** 533–544.

Ishii, T., and Yanagida, M. (1977). The two dispensable structural proteins (soc and hoc) of the T4 phage capsid; their purification and properties, isolation and characterization of the defective mutants, and their binding with the defective heads in vitro. *J. Mol. Biol.* **109,** 487–514.

Jiang, J., Abu-Shilbayeh, L., and Rao, V. B. (1997). Display of a PorA peptide from *Neisseria meningitidis* on the bacteriophage T4 capsid surface. *Infect. Immun.* **65,** 4770–4777.

Johnson, K., Condie, B., Mooney, D. T., and Doermann, A. H. (1992). Mutations that eliminate the requirement for the vertex protein in bacteriophage T4 capsid assembly. *J. Mol. Biol.* **224,** 601–611.

Kellenberger, E. (1990). Form determination of the heads of bacteriophages. *Eur. J. Biochem.* **190,** 233–248.

Kistler, J., Aebi, U., Onorato, L., ten, Heggeler, B., and Showe, M. K. (1978). Structural changes during the transformation of bacteriophage T4 polyheads: Characterization of the initial and final states by freeze-drying and shadowing Fab-fragment-labelled preparations. *J. Mol. Biol.* **126,** 571–589.

Laemmli, U. K. (1970). Cleavage of structural proteins during the assembly of the head of bacteriophage T4. *Nature* **227,** 680–685.

Lane, T., and Eiserling, F. A. (1990). Genetic control of capsid length in bacteriophage T4 VII. A model of length regulation based on DNA size. *J. Struct. Biol.* **104,** 9–23.

Laue, T. M., Shah, B. D., Ridgeway, T. M., and Pelletier, S. L. (1992). *In*: "Analytical Ultracentrifugation in Biochemistry and Polymer Science" (S. E.Harding, A. J. Rowe, and J. C. Horton, Eds.), pp. 90–125. Royal Society for Chemistry.

Leibo, S. P., Kellenberger, E., Kellenberger-van der Kamp, C., Frey, T. G., and Steinberg, C. M. (1979). Gene 24-controlled osmotic shock resistance in bacteriophage T4: Probable multiple gene functions. *J. Virol.* **30,** 327–338.

MacDonald, P. M., Kutter, E., and Mosig, G. (1984). Regulation of a bacteriophage T4 late gene, soc, which maps in the early regions. *Genetics* **106,** 17–27.

Maniatis, T. Fritsch, E. F. and Sambrook, J. (1982). Molecular Cloning: A Laboratory Manual. Cold Spring Harbor Press, Cold Spring Harbor, NY.

McNicol, A. A., Simon, L. D., and Black, L. (1977). A modulation which bypasses the requirement for p24 in bacteriophage T4 capsid morphogenesis. *J. Mol. Biol.* **116,** 261–283.

Moody, M. F. (1999). Geometry of phage head construction. *J. Mol. Biol.* **293,** 401–433.

Mooney, D. T., Stockard, J., Parker, M. L., and Doermann, A. H. (1987). Genetic control of capsid length in bacteriophage T4: DNA sequence analysis of petite and petite/giant mutants. *J. Virol.* **61,** 2828–2834.

Mullaney, J. M., and Black, L. W. (1998). Activity of foreign proteins targeted within the bacteriophage T4 head and prohead: Implications for packaged DNA structure. *J. Mol. Biol.* **283,** 913–929.

Müller-Salamin, L., Onorato, L., and Showe, M. K. (1977). Localization of minor protein components of the head of bacteriophage T4. *J. Virol.* **24,** 121–134.

Onorato, L., and Showe, M. K. (1975). Gene 21 protein-dependent proteolysis in vitro of purified gene 22 product of bacteriophage T4. *J. Mol. Biol.* **92,** 395–412.

Onorato, L., Stirmer, B., and Showe, M. K. (1978). Isolation and characterization of bacteriophage T4 mutant preheads. *J. Virol.* **27,** 409–426.

Perczel, A., Park, K, and Fasman, G. D. (1990). Analysis of the circular dichroism spectrum of proteins using the convex constraint algorithm: A practical guide (1992). *Anal. Biochem.* **203,** 83–93.

Rao, V. B., and Black, L. W. (1988). Cloning, overexpression and purifi-

cation of the terminase proteins gp16 and gp17 of bacteriophage T4: Construction of a defined in vitro DNA packaging system using purified terminase proteins. *J. Mol. Biol.* **200,** 475–488.

Ren, Z.-J., and Black, L. W. (1998). Phage T4 Soc and Hoc display of biologically active full-length proteins on the viral capsid. *Gene* **215,** 439–444.

Ren, Z. J., Lewis, G. K., Wingfield, P. T., Locke, E. G., Steven, A. C., and Black, L. W. (1996). Phage display of intact domains at high copy number: A system based on SOC, the small outer capsid protein of bacteriophage T4. *Protein Sci.* **5,** 1833–1843.

Ross, P. D., Black, L. W., Bisher, M. E., and Steven, A. C. (1985). Assembly-dependent conformational changes in a viral capsid protein. Calorimetric comparison of successive conformational states of the gp23 surface lattice of bacteriophage T4. *J. Mol. Biol.* **183,** 353–364.

Saxton, W. O., and Baumeister, W. (1982). The correlation averaging of a regularly arranged bacterial cell envelope protein. *J. Microsc. (Oxford)* **127,** 127–138.

Showe, M. K., and Onorato, L. (1978). Kinetic factors and form determination of the head of bacteriophage T4. *Proc. Natl. Acad. Sci. USA* **75,** 4165–4169.

Sreerama, N., and Woody, R. W. (1993). A self-consistent method for the analysis of protein secondary structure from circular dichroism. *Anal. Biochem.* **209,** 32–44.

Sternberg, N., and Weisberg, R. (1977). Packaging of coliphage lambda DNA. II. The role of the gene D protein. *J. Mol. Biol.* **117,** 733–759.

Steven, A. C., Couture, E., Aebi, U., and Showe, M. K. (1976). Structure of T4 polyheads. II. A pathway of polyhead transformation as a model for T4 capsid maturation. *J. Mol. Biol.* **106,** 187–221.

Steven, A. C., Greenstone, H. L., Booy, F. P., Black, L. W., and Ross, P. D. (1992). Conformational changes of a viral capsid protein: Thermodynamic rationale for proteolytic regulation of bacteriophage T4 capsid expansion, cooperativity, and super-stabilization by Soc binding. *J. Mol. Biol.* **228,** 870–884.

Tao, Y., Olson, N. H., Xu, W., Anderson, D. L., Rossmann, M. G., and Baker, T. S. (1998). Assembly of a tailed bacterial virus and its genome release studied in three dimensions. *Cell* **95,** 431–437.

Towbin, H., Staehelin, T., and Gordon, J. (1979). Electrophoretic transfer of proteins from polyacrylamide gels to nitrocellulose sheets: Procedure and some applications. *Proc. Nat'l. Acad. Sci. USA* **76,** 4350–4354.

Trus, B. L., Kocsis, E., Conway, J. F., and Steven, A. C. (1996). Digital image processing of electron micrographs: The PIC system-III. *J. Struct. Biol.* **116,** 61–67.

Trus B. L., Rao, V., Cheng, N., and Steven, A. C. (1997). Molecular architecture of isometric capsids of bacteriophage T4. 15th Int'l. Conf. On Phage and Virus Assembly, Asilomar, CA. (Abstr.).

van Driel, R. (1980). Assembly of bacteriophage T4 head-related structures. IV. Isolation and association properties of T4 prehead proteins. *J. Mol. Biol.* **138,** 27–42.

Wetlaufer, D. B. (1962). Ultraviolet spectra of proteins and amino acids. *Adv. Prot. Chem,* **17,** 303–390.

Wingfield, P. T., Mattallano, R. J., MacDonald, H. R., Craig, S., Clore, G. M., Gronenbom, A. M., and Schmelssner, U. (1987). *Prot. Eng.* **1,** 413–417.

Yang, F, Forrer, P., Dauter, Z., Conway, J. F., Cheng, N., Cerritelli M. E., Steven, A. C., Plückthun, A., and Wlodawer, A. (2000). Novel fold, and capsid-binding properties of the λ phage display platform protein gpD. *Nat. Struct. Biol.* **7,** 230–237.